Low-field hysteresis in the magnetoimpedance of amorphous microwires

M. Ipatov,* V. Zhukova, A. Zhukov, J. Gonzalez, and A. Zvezdin†
Departamento de Física de Materiales, Facultad de Qímicas, Universidad del País Vasco, San Sebastián, Spain
(Received 14 January 2010; revised manuscript received 8 March 2010; published 19 April 2010)

The phenomena of low-field hysteresis of the magnetoimpedance (MI) in zero-magnetostrictive amorphous wires are studied theoretically and experimentally. We developed a mathematical model for magnetization reversal and impedance field dependence. The presented model considers the low-field hysteresis and the effect of circular bias magnetic field. It is demonstrated that the hysteresis originates from a nonzero angle α between the anisotropy easy axis and transversal plane. The bias field, which is produced by current running through the wire, considerably affects the MI dependence making it anhysteretic and highly asymmetric. The validity of the model is confirmed by the experiments. The main characteristics of the studied amorphous wire such as anisotropy field H_A, angle between the anisotropy easy axis with the transversal direction α, and Gilbert damping constant α_G were obtained from the experiment in accordance with the presented model.

DOI: 10.1103/PhysRevB.81.134421 PACS number(s): 75.47.−m, 75.30.Gw, 75.50.Kj, 75.60.Jk

I. INTRODUCTION

The giant magnetoimpedance effect (GMI) consists of significant change of the impedance of a magnetically soft conductor upon the application of an external magnetic field. The GMI effect is intrinsically related with magnetic softness and requires low magnetic anisotropy constant and high circumferential magnetic permeability. In particular, these conditions are fulfilled in magnetically soft amorphous wires with low and negative magnetostriction constant ($\lambda_s \approx -10^{-7}$).[1] It was reported the sensitivity to magnetic field as high as 1 μOe (Ref. 2) and up to hundreds of percents of the impedance changes in amorphous wires[1,3,4] that, combined with low cost and simple fabrication method, have made them very attractive for prospective application where localized weak magnetic field is especially important such as biomedical, geological, environmental, navigation, and industrial highly sensitive magnetic field sensing.

Recently a novel family of amorphous wires with reduced dimensionality—glass-coated microwires consisting on much thinner metallic ferromagnetic nucleus (usually of the order of 1–30 μm) coated by glass—has been developed.[4,5] These microwires fit much better for utilization in magnetic sensors mostly because of their thinner dimensions and therefore lower effect of demagnetizing stray fields. At certain conditions such microwires exhibit quite good magnetic softness, high GMI (Refs. 5 and 6) and stress-impedance[7] effects.

Another emerging application of amorphous microwires is tunable and self-sensing composite materials with microwave electromagnetic properties depending on the impedance of the microwires embedded in the dielectric matrix.[8–12] The use of microwires with high GMI and stress impedance effects in composites gives the possibility to realize the materials which dielectric permittivity is determined by the structural scaling, external stimuli or internal state of the material. For example, a material with self-monitoring properties could be able to evidence invisible structural damages, defects, excessive loadings, local stress, and temperature distribution, thus considerably facilitating the *in situ* health monitoring of large scale objects such as infrastructure (bridges, buildings, etc.).

Obviously, for both GMI applications in magnetic field sensors and tunable composites, the highly sensitive MI and its low hysteresis are required. Consequently, improvement of these parameters is essential for these applications. At the same time, the hysteresis up to 100 A/m or even higher was found in amorphous microwires[13] that considerably limit the sensor's precision.[14]

Though the MI effect has been rather extensively studied over the last two decades, most of the performed investigations were devoted to MI in high fields (above 1 kA/m). To the best of our knowledge, the problem of low-field hysteresis in amorphous wires was consider only in a few works.[15,16] It these papers it was shown that the MI hysteresis is related with static circumferential magnetization and the application of circumferential dc bias field H_B is required to suppress this hysteresis. Nevertheless, a complete model describing all aspects of MI dependence such as hysteresis, asymmetry induced by the bias field, influence of anisotropy constant, and so on has not been given. Thus, rigorous theoretical and experimental studies of MI effect with consideration for the low-field anomalies are of considerable interest and importance.

In the paper we developed the mathematical model for the magnetization reversal and MI field dependence for zero-magnetostrictive amorphous microwires and compared it with the experiment. The paper is organized as follows. First, we considered the equilibrium magnetization state in the surface layer of the wire. We assume (i) a nonzero angle between the anisotropy easy axis and transversal plane and (ii) the presence of a dc circular field that is created by the bias current. Second, the tensors of magnetic permeability and surface impedance are discussed. Finally, the model is compared with the experimental measurements from which the main characteristics of the microwire such as anisotropy field H_A, angle between the anisotropy easy axis with the transversal direction α, and Gilbert damping constant α_G were obtained.

II. MAGNETIC STRUCTURE

The outer shell of amorphous glass-coated microwires with vanishing magnetostriction is characterized by the cir-

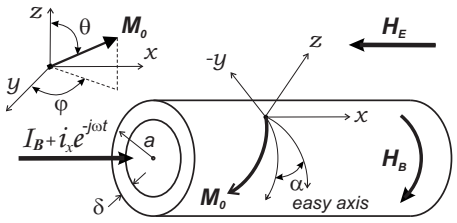

FIG. 1. Principal directions in microwire.

cular magnetization that can be divided into magnetic domains forming bamboolike structures. However, the bamboo domain structure in the outer shell is unfavorable for short and uniform samples having low magnetostriction.[17] But even if the bamboo domain structure is present, the application of a sufficiently high circular magnetic field H_B will eliminate it. Therefore, we can assume that the outer shell, where the high-frequency current is concentrating due to skin effect, is a single domain particle. Also, at high frequencies (well above 1 MHz), the domain-wall motion is severely dumped by the eddy currents and magnetic-moment rotation is the dominant mechanism responsible for the MI.[18]

For further analysis, it is convenient to introduce the local coordinate system situated at arbitrary point on the surface as shown in Fig. 1 where x axis is parallel to the wire's longitudinal axis; y and z are tangent and normal components. Here, θ and φ are the polar and azimuthal angles of the magnetization vector M_0 in this local coordinate system.

Magnetic characterization of the surface magnetic shell can be naturally performed in according with classical electrodynamics in terms of the multipole expansion of magnetization (or the Ampere's currents) distribution that involves the following components:

(i) dipole magnetic moment $\vec{M}=(M_x,0,0)$, $M_x=M_s \sin\theta \sin\varphi \approx M_s \sin\varphi$;

(ii) toroidal magnetic moment $\vec{T}=1/2\Sigma[\vec{r}\times\overrightarrow{M_{surf}}]$. Evidently $\vec{T}=(\tau,0,0)$ where $\tau=\pi a M_s \delta \sin\theta \cos\varphi = \pi a M_s \delta \cos\varphi$, a is the wire radius, and δ is the thickness of the outer shell (Fig. 1);

(iii) the components of the quadruple magnetic moment $D=\Sigma M_x r_x$ which pulls the spins out-of-plane tangential to the surface. They are described by a small angle $\Delta\theta=\pi/2-\theta$. In equilibrium $D=0$ but in dynamics: $D_{zz}=\Sigma M_z r_r = M_s a 2\pi\Delta\theta$.

Thereby, the local angles θ and φ completely describe the equilibrium magnetization distribution and dynamics of the studied system. We consider below the coherent remagnetization processes; i.e., the local angles θ and φ are the same in all points of the surface shell. Obviously, in the laboratory coordinate system the orientations of the magnetic vectors are different in different points of the surface due to its curvature. The condition of feasibility of this assumption is defined by the following inequality:

$$a \gg L_m, \tag{1}$$

where $L_m=\sqrt{A/2\pi M_s^2}$ is the characteristic magnetic length.

The dynamics of the studied magnetic system is governed by Landau-Lifshitz equations with the following Lagrangian function:

$$L=\frac{M_S}{\gamma}(1-\cos\theta)\dot{\varphi}-U(\theta,\varphi) \tag{2}$$

and the dissipative Rayleigh function,

$$R=\frac{\alpha_G M_s}{2\gamma}(\dot{\theta}^2+\sin^2\theta\dot{\varphi}^2), \tag{3}$$

where $\gamma=2\mu_b/\hbar$ is the gyromagnetic ratio, α_G is the dimensionless Gilbert damping constant, and $U(\theta,\varphi)$ is the total magnetic energy of the system.

III. EQUILIBRIUM MAGNETIZATION STATE

The total energy U can be expressed as the sum of magnetostatic energy, energy of magnetic anisotropy, Zeeman energy, and the energy supplied by the circular bias magnetic field,

$$U(\theta,\varphi)=-K_1\sin^2\theta+K_A\sin^2\theta\sin^2(\varphi+\alpha) - M_s H_E \sin\theta\sin\varphi+M_s H_B \sin\theta\cos\varphi, \tag{4}$$

where $K_1=2\pi M_s^2$, θ and φ are the polar and azimuthal angle of the magnetization vector, α is the angle between the anisotropy easy axis with the transversal direction (see Fig. 1), K_A is the anisotropy constant, H_E is the external magnetic field applied along the x axis, and H_B is dc bias field that is produced by the current I_B running through the wire.

The minimum of the total energy U is achieved when $\theta=\pi/2$ (i.e., the magnetization vector is parallel to the surface of the cylinder). Then Eq. (4) minimizes to

$$U(\theta=\pi/2,\varphi)=K_A\sin^2(\varphi+\alpha)-M_s H_E\sin\varphi+M_s H_B\cos\varphi. \tag{5}$$

The magnetization orientation can be found by minimization of the total energy U over the angle φ. The equilibrium angle φ_0 between the magnetization vector and the transversal direction is calculated from Eq. (5) as $dU/d\varphi=0$,

$$2H_E\cos\varphi_0=H_A\sin 2(\varphi_0+\alpha)+2H_B\sin\varphi_0, \tag{6}$$

where $H_A=2K_A/M_s$ is the surface anisotropy field. Equation (6) describes the rotation of magnetization vector under the applied magnetic field H_E.

The magnetization reversal process in the system with arbitrary angle between the anisotropy easy axis and direction of applied magnetic field is described by the Stoner-Wohlfarth model.[19] Figure 2 shows the solution of Eq. (6) as function $\varphi_0(H_E)$ for angle $\alpha=30°$ and for two value of bias field H_B of 0.3 H_A and 0.5 H_A. The dependence $\varphi_0(H_E)$, shown in Fig. 2(a), is hysteretic. Increasing the bias field up to 0.5 H_A results in the disappearance of the hysteresis, as it can be seen from the dependence in Fig. 2(b).

Knowing the dependence $\varphi_0(H_E)$, the longitudinal magnetization component M_x (magnetization projection on x axis) can be easily obtained as

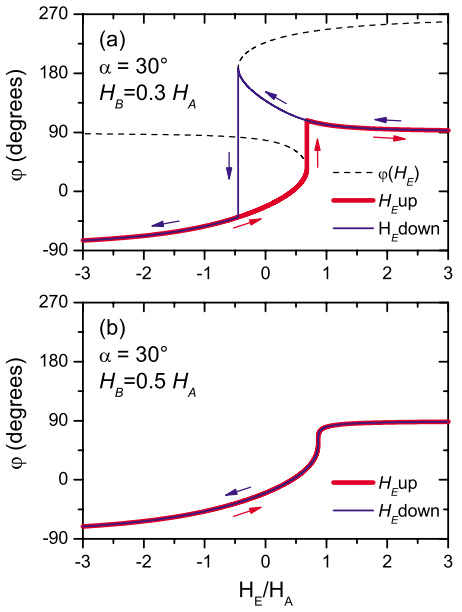

FIG. 2. (Color online) $\varphi_0(H_E)$ with α and H_B as parameters.

$$M_x = M_s \sin \varphi_0, \tag{7}$$

which is shown in Fig. 3 for different values of α and H_B. When $H_B=0$ [Fig. 3(a)], the $M_x(H_E)$ dependence is an hysteretic if $\alpha=0$ and with hysteresis if α is not zero which is consistent with the Stoner-Wohlfarth model. With application of H_B, the hysteresis is not observed at $\alpha=10°$ and $H_B=0.3$ H_A [Fig. 3(b)] and at $\alpha=30°$ and $H_B=0.5$ H_A[Fig. 3(c)] as $\arcsin(0.3)=17.4°$ and $\arcsin(0.5)=30°$. To suppress the hysteresis when $\alpha=50°$, the bias field as high as $\sin(50°)=0.77$ H_A will be required. Therefore, we can conclude that the hysteresis of $\varphi_0(H_E)$ and $M_x(H_E)$ originates from the easy axis's deviation from circular direction and can be suppressed by applying the bias field $H_B > H_A \cdot \sin \alpha$.

IV. TENSORS OF MAGNETIC PERMEABILITY AND SURFACE IMPEDANCE

The Landau-Lifshitz equations for magnetization dynamics in spherical coordinates read as

$$\dot{\theta} + \alpha_G \sin \theta \dot{\varphi} = \gamma H_\varphi$$

$$\alpha_G \dot{\theta} - \sin \theta \dot{\varphi} = \gamma H_\theta, \tag{8}$$

where

$$H_\varphi = -(\mu_0 M_s \sin \theta)^{-1} \frac{\partial U}{\partial \varphi} = H_A \sin \theta \sin 2(\varphi + \alpha) - H_E \cos \varphi + H_B \sin \varphi,$$

$$H_\theta = -(\mu_0 M_s)^{-1} \frac{\partial U}{\partial \theta} = -(2K_1/M_s)\sin \theta \cos \theta + H_A \sin 2\theta \sin^2(\varphi + \alpha) - H_E \cos \theta \sin \varphi - H_B \cos \theta \cos \varphi \tag{9}$$

Let us represent θ and φ as

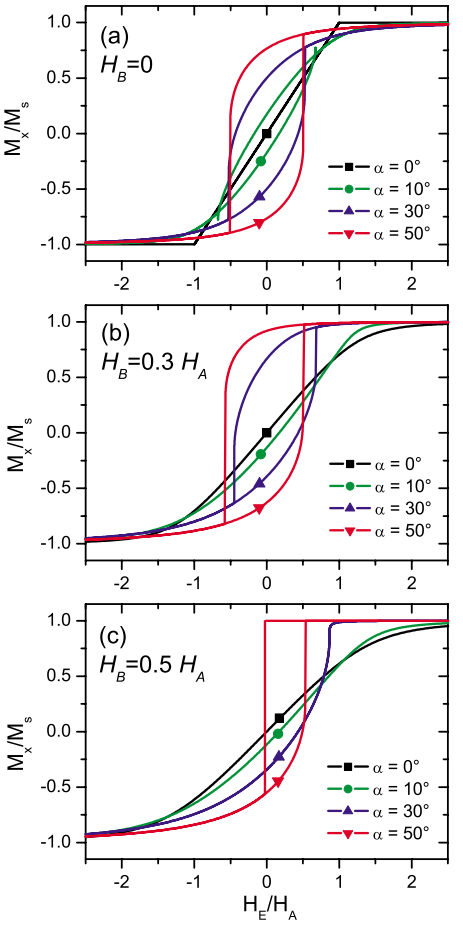

FIG. 3. (Color online) $M_x(H_E)$ with α and H_B as parameters.

$$\theta = \theta_0 + \theta_1, \quad \varphi = \varphi_0 + \varphi_1, \tag{10}$$

where θ_0 and φ_0 are the equilibrium values and θ_1 and φ_1 are the small ones describing the magnetization precession under the high-frequency magnetic field, which can be found from the following linear equation:

$$\dot{\theta}_1 + \alpha_G \sin \theta \dot{\varphi}_1 = \gamma(H_{\varphi\varphi}\varphi_1 + H_{\varphi\theta}\theta_1)$$

$$\alpha_G \dot{\theta}_1 - \sin \theta \dot{\varphi}_1 = \gamma(H_{\theta\varphi}\varphi_1 + H_{\theta\theta}\theta_1), \tag{11}$$

where

$$H_{\varphi\varphi} = \frac{\partial H_\varphi}{\partial \varphi} = H_A \sin \theta \cos 2(\varphi + \alpha) + H_E \sin \varphi + H_B \cos \varphi,$$

$$H_{\varphi\theta} = \frac{\partial H_\varphi}{\partial \theta} = H_{\theta\varphi} = \frac{\partial H_\theta}{\partial \varphi} = H_A \sin 2\theta \sin 2(\varphi + \alpha) - H_E \cos \theta \cos \varphi + H_B \cos \theta \sin \varphi,$$

$$H_{\theta\theta} = \frac{\partial H_\theta}{\partial \theta} = -\frac{2K_1}{M_s}\cos 2\theta + H_A \cos 2\theta \sin^2(\varphi + \alpha) + H_E \sin \theta \sin \phi + H_B \sin \theta \sin \varphi. \tag{12}$$

Assuming that $\theta_1(t)=\theta_1 e^{-i\omega t}$, $\varphi_1(t)=\varphi_1 e^{-i\omega t}$ and $h_x(t)=h_x e^{-i\omega t}$, $h_y(t)=h_y e^{-i\omega t}$ are the axial and circumferential mag-

netic fields excited by the harmonic current i_x with frequency ω flowing trough the wire, then

$$-i\omega\theta_1 + (\gamma H_{\varphi\varphi} - i\alpha_G\omega)\varphi_1 = -\gamma(-h_y(t)\cos\varphi_0 + h_y(t)\sin\varphi_0)$$

$$(-i\alpha_G\omega - \gamma H_{\theta\theta})\theta_1 + i\omega\varphi_1 = 0. \quad (13)$$

Then, solutions for θ_1 and φ_1 are as follows:

$$\theta_1 = \frac{i\omega\gamma}{D(\omega)}[h_x(t)\cos\varphi_0 + h_y(t)\sin\varphi_0] \quad (14)$$

$$\varphi_1 = -\frac{i\omega_M\gamma}{D(\omega)}[h_x(t)\cos\varphi_0 + h_y(t)\sin\varphi_0] \quad (15)$$

where

$$D(\omega) = \omega^2 - \omega_0^2 - i\alpha_G\omega\omega_M, \quad (16)$$

$$\omega_M = \gamma\mu_0(H_{\varphi\varphi} + H_{\theta\theta}) \approx \gamma\mu_0 H_{\theta\theta} \approx \gamma\mu_0 M_s, \quad (17)$$

$$\omega_0^2 = \gamma^2(H_{\varphi\varphi}H_{\theta\theta} - H_{\varphi\theta}^2) \approx \omega_M(\omega_A\cos 2(\varphi+\alpha) + \omega_E\sin\varphi + \omega_B\cos\varphi), \quad (18)$$

and $\omega_A = \gamma H_A$, $\omega_E = \gamma H_E$, and $\omega_B = \gamma H_B$.

Substituting θ and φ in the formulas for magnetization,

$$M_x = M_s\sin\theta\sin\varphi$$

$$M_y = M_s\sin\theta\cos\varphi \quad (19)$$

and $\theta = \pi/2$, one can get the susceptibility and permeability tensors,[15]

$$\chi_{xx} = \omega_M^2\cos^2\varphi/D(\omega) = \tilde{\mu}\cos^2\varphi$$

$$\chi_{xy} = \omega_M^2\sin\varphi\cos\varphi/D(\omega) = \tilde{\mu}\sin\varphi\cos\varphi$$

$$\chi_{yx} = \omega_M^2\sin\varphi\cos\varphi/D(\omega) = \tilde{\mu}\sin\varphi\cos\varphi$$

$$\chi_{yy} = \omega_M^2\sin^2\varphi/D(\omega) = -\tilde{\mu}\sin^2\varphi \quad (20)$$

$$\mu_{xx} = 1 + \tilde{\mu}\cos^2\varphi$$

$$\mu_{xy} = \mu_{yx} = \tilde{\mu}\sin\varphi\cos\varphi$$

$$\mu_{yy} = 1 + \tilde{\mu}\sin^2\varphi \quad (21)$$

$$\tilde{\mu} = \frac{\omega_M^2}{\omega_0^2(\varphi) - i\alpha_G\omega\omega_M - \omega^2}. \quad (22)$$

The surface impedance tensor can be obtained by solving Maxwell equation with proper boundary conditions. The theoretical solutions of surface impedance tensor for ferromagnetic body of cylindrical shape were performed by Antonov *et al.*,[15] Usov *et al.*,[20] Panina *et al.*[16] The general solution of this task is rather bulky. It is expressed in terms of series of δ/a. If the magnetic permeability μ is rather high (in our samples μ reaches 10^5), the high-frequency approximation ($\delta \ll a$) can be used. Therefore, the surface impedance tensor components Z_{zz} and $Z_{\varphi z}$ can be expressed by the following formulas:[15]

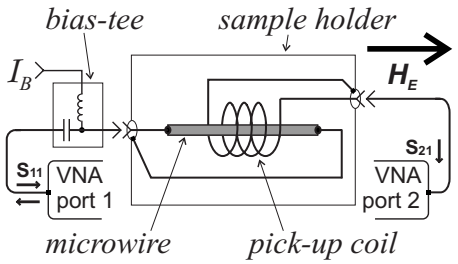

FIG. 4. Schematic of the experimental setup for measuring the impedance matrix elements Z_{zz} and $Z_{\varphi z}$.

$$Z_{zz} = \frac{u_x}{i_x} = \frac{e_x(a)l}{i_x} = \sqrt{\frac{\mu_0\rho\omega}{2i}}(\sqrt{\tilde{\mu}+1}\sin^2\varphi + \cos^2\varphi)\frac{l}{2\pi a}, \quad (23)$$

$$Z_{\varphi x} = \frac{e_\varphi}{i_x} = \sqrt{\frac{\mu_0\rho\omega}{2i}}(\sqrt{\tilde{\mu}+1} - 1)\sin\varphi\cos\varphi) \quad (24)$$

where u_x is the voltage drop along the wire, e_x and e_φ are electric-field components, a and l are the wire radius and length, and ρ is the electric resistivity.

V. COMPARISON WITH THE EXPERIMENT

We have studied the MI effect in as-cast nearly zero-magnetostrictive amorphous glass-coated microwire. The microwire with nominal composition $Co_{67.1}Fe_{3.8}Ni_{1.4}Si_{14.5}B_{11.5}Mo_{1.7}$ was fabricated by Taylor-Ulitovsky method;[21] it has the amorphous core diameter d of 21.4 μm and the glass coating thickness of 2.4 μm. The sample length l is 6 mm.

We measured the longitudinal diagonal Z_{zz} and off-diagonal $Z_{\varphi z}$ components of the impedance tensor with a vector network analyzer (VNA) and compared them with the model. The schematic of the experimental setup is shown in Fig. 4. The microwire was soldered in a specially designed microstrip cell. One wire end was connected to the inner conductor of a coaxial line through a matched microstrip line while the other was connected to the ground plane. The dc bias current I_B was applied to the sample through a bias-tee element. The sample holder was placed inside a sufficiently long solenoid that creates a homogeneous magnetic field H_E in the sample. All measurements were done at frequency of 10 MHz.

The Z_{zz} component was measured through the reflection coefficient S_{11} as $Z_{zz} = Z_0(1+S_{11})(1-S_{11})$, $Z_0 = 50\ \Omega$ is the characteristic impedance of the coaxial line. The high-frequency current i_x passing through the wire creates a circumferential magnetic field h_φ. As the permeability is a tensor value with nonzero off-diagonal terms, the precision of h_φ causes the appearance of m_x. Then, in accordance with Faraday's law, the variation in m_x induces a voltage in the pick-up coil wounded on the wire. In this way, the $Z_{\varphi z}$ com-

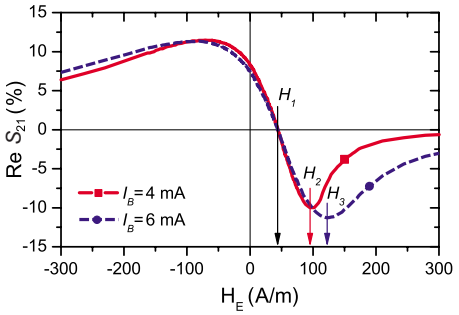

FIG. 5. (Color online) The experimental dependence of $Z_{\varphi z} \propto S_{21}$ on external magnetic field with I_B as a parameter.

ponent can be found through transmission coefficient S_{21} which is the ratio of the signal induced in the ten turns pick-up coil to the constant generator voltage applying to the wire.

Two-step calibration procedure was applied. First a standard short-open-load-thru calibration sets the reference plane at the cables ends (after the bias tee for port 1). Then, the serial and parallel parasitics associated with the sample holder were removed from the measurements. The parasitics were found from open and short measurement of the empty sample holder.

Equation (6) contains three unknown constants H_A, α, and H_B which, considering Eq. (24), can be extracted from the experimental data. In the $Z_{\varphi z}(H)$ graph shown in Fig. 5, one can obtain the characteristic points that will allow calculating the unknown constants:

(1) when $\varphi=0$, there is no magnetization precession along the x axis and, therefore, no signal is induced in the pick-up coil. The corresponding magnetic field H_1 is 42 A/m for both curves.

(2) On the other hand, according to Eq. (24), Re $Z_{\varphi z}$ is proportional to (Im $\tilde{\mu}$)sin φ cos φ and the induced voltage is maximal when $\varphi=\pi/4$. As shown in Fig. 10(b), the minimum (negative peak) of Re $Z_{\varphi z}$ is actually defined by the minimum of sin φ cos φ as (Im $\tilde{\mu}$) has maximum at this point. Here the magnetic field H_2 is 96 A/m at I_B=4 mA (solid curve in Fig. 5).

(3) Changing I_B (and therefore H_B) we can find the third point required to solve Eq. (6). Here the $\varphi=\pi/4$ at minimum of Re $Z_{\varphi z}$ as in previous case, but we increase I_B to 6 mA (dashed curve in Fig. 5) which resulted in shifting the field with maximum induced emf to H_3 of 120 A/m.

The solution of Eq. (6) for two φ angles,

$$\begin{aligned} &\varphi = 0 && 2H_1 = H_A \sin 2\alpha \\ &\varphi = \pi/4, H_{B1} && \sqrt{2}H_2 = H_A \cos 2\alpha + \sqrt{2}H_{B1} \\ &\varphi = \pi/4, H_{B2} && \sqrt{2}H_3 = H_A \cos 2\alpha + \sqrt{2}H_{B2}, \end{aligned} \tag{25}$$

where $H_{B2}=1.5H_{B1}$, gives the following value of the constants: $H_A=108$ A/m, $\alpha=25.5°$, and $H_{B1}=48$ A/m when $I_B=4$ mA. The found value of the anisotropy field H_A of 108 A/m confirms the high magnetic softness of the sample. On the other hand, the angle of helical anisotropy $\alpha=25.5°$ is surprisingly high.

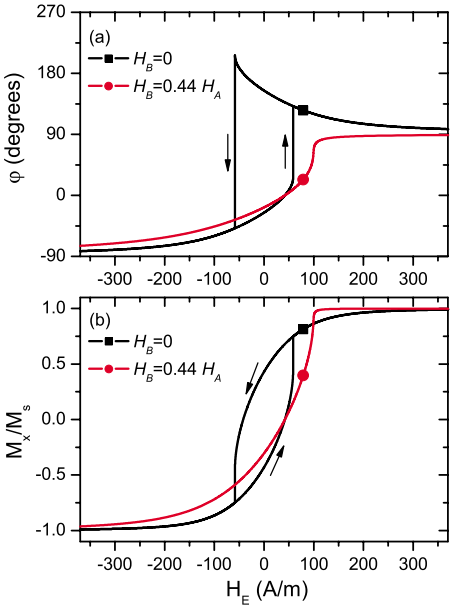

FIG. 6. (Color online) $\varphi_0(H_E)$ and $M_x(H_E)$ with H_B as a parameter. Modeling is performed for wires with $H_A=108$ A/m and $\alpha=25.5°$.

Further we substituted $H_A=108$ A/m and $\alpha=25.5°$ in Eqs. (6) and (7) and obtained the modeled dependencies $\varphi_0(H_E)$ and $M_x(H_E)$ for the studied sample which are presented in Fig. 6. As one can see, without the bias field H_B, the surface magnetization M_x exhibits hysteresis with coercitivity field of 41 A/m. The hysteresis disappears when the bias field is applied.

Now, to calculate the MI dependencies the Gilbert damping constant α_G is requires. This parameter is usually defined from ferromagnetic-resonance experiments at high field and high frequency. The reported values widely spread from 0.01 to 0.1. We calculated the MI dependencies Z_{zz} and $Z_{\varphi z}$ for different α_G and showed them in Fig. 7 together with the experimental measurement. As it is seen from the graphs, the damping constant α_G greatly affects the MI curves. From fitting we took $\alpha_G=0.012$.

Substituting the found values for H_A, α, and α_G in Eqs. (22)–(24), we obtained the calculated MI dependencies and compared it with the experimental data that are shown in Figs. 8 and 9 for Z_{zz} and $Z_{\varphi z}$, respectively. The agreement of the model with experiment is satisfactory. The developed model correctly describes the hysteresis of the MI and the asymmetry induced by H_B. In the absence of the bias field, both dependencies Z_{zz} and $Z_{\varphi z}$ exhibit hysteresis. Nevertheless, the off-diagonal component $Z_{\varphi z}$ [Fig. 9(a)] is rather high, which confirms the single domain state of the outer shell. Otherwise, the division of domain with formation of bamboolike stricture would have resulted in almost zero response as the contribution of domain with antiparallel magnetization would cancel each other.[22] The application of the bias field H_B makes the dependencies anhysteretic with a high sensitivity dZ/dH slope. It worth noting that if the pulse current excitation is applied, the use of a separate bias current is not required since the pulse already contains the dc component.

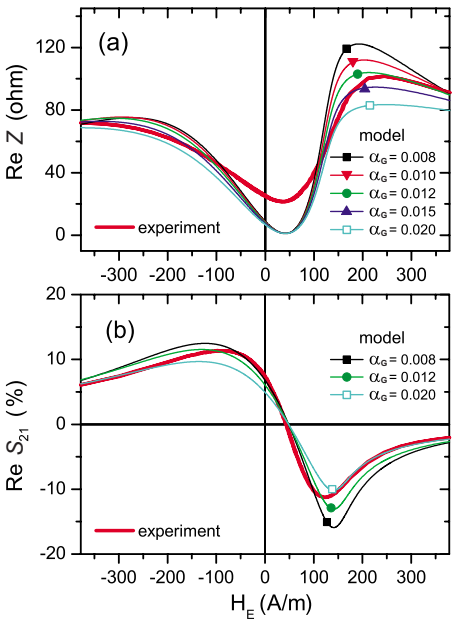

FIG. 7. (Color online) Fitting Gilbert damping constant α_G to experimental data, H_B=0.66H_A.

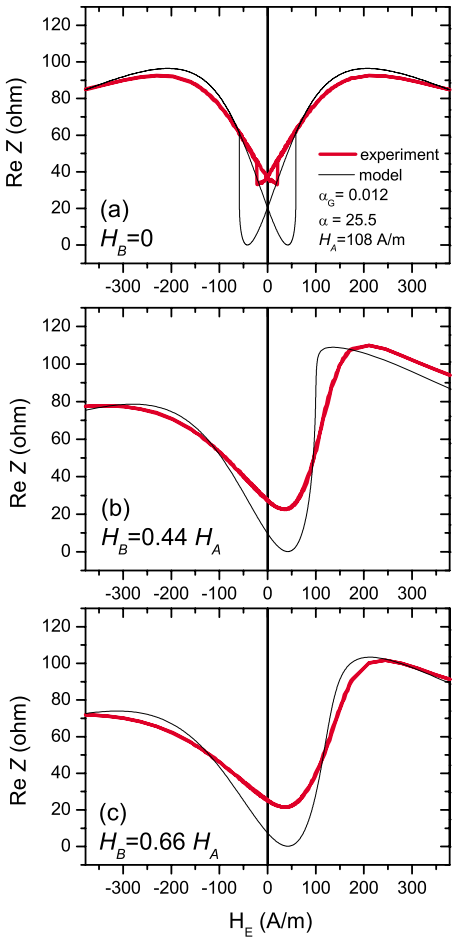

FIG. 8. (Color online) Experimental measurement of Z_{zz} and comparison with the model.

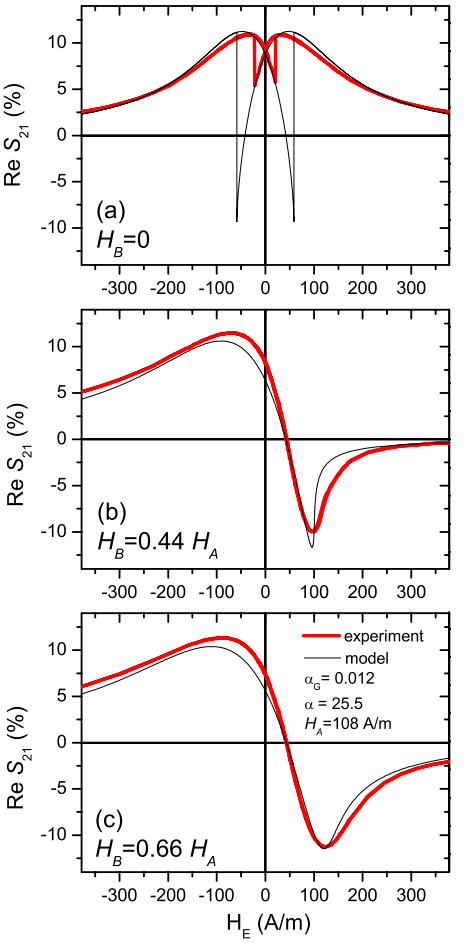

FIG. 9. (Color online) Experimental measurement of $Z_{\varphi z}$ and comparison with the model.

The calculated field dependence of the real parts of Z_{zz} and $Z_{\varphi z}$ for H_B=0.44H_A is shown in Fig. 10. These dependences, conforming to Eqs. (23) and (24), are composed of two components: (i) $\sin^2\varphi$ for Z_{zz} and $\sin\varphi\cos\varphi$ for $Z_{\varphi z}$ and (ii) Im μ. As one can see, at low field below H_A, the shape of the MI tensor components is mainly determined by the angle φ while the permeability defines the maximum value of MI tensor components. At fields above H_A, φ approaches $\pi/2$ [see Fig. 6(a)], therefore $\sin^2\varphi \to 1$, Z_{zz} slowly decreases with the permeability as the sample is reaching the saturated state. The off-diagonal component $Z_{\varphi z}$ rapidly falls to zero at high fields, as $\sin\varphi\cos\varphi \to 0$.

Let us consider, following Kraus,[23] the theoretical maximum for GMI effect for the studied microwire. Equation (23) can be transformed to

$$\frac{Z_{zz}}{R_{dc}} = (1+i)\left(\frac{\sin^2\varphi}{\delta} + \frac{\cos^2\varphi}{\delta_0}\right)a \tag{26}$$

where R_{dc} is the wire's dc resistance and δ and δ_0 are magnetic and nonmagnetic skin depths,

$$\delta = \sqrt{\frac{2\rho}{\mu_0\omega(\tilde{\mu}+1)}}, \quad \delta_0 = \sqrt{\frac{2\rho}{\mu_0\omega}}. \tag{27}$$

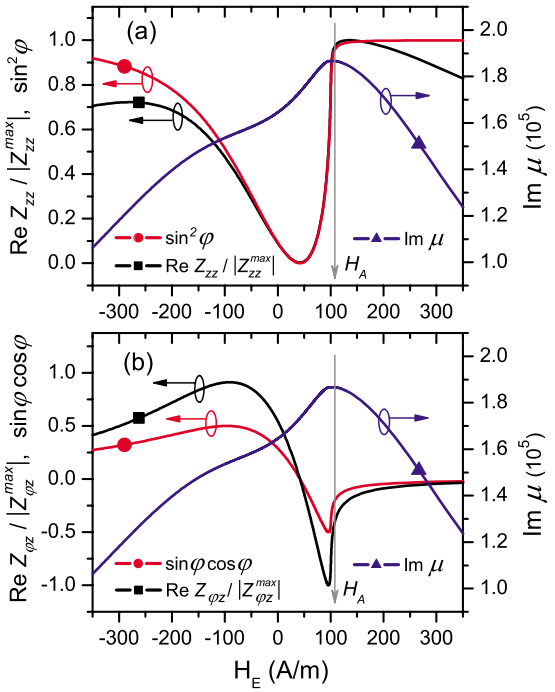

FIG. 10. (Color online) Real parts of Z_{zz} and $Z_{\varphi z}$ which are defined by multiplication of (Im μ) and $\sin^2\varphi$ and $\sin\varphi\cos\varphi$, respectively. Modeling is performed with parameters $\alpha=25.5°$, $H_A=108$ A/m, and $H_B=0.44H_A$.

The theoretical minimum of the skin depth is reached when $\omega=\omega_0$,

$$\delta_{min}=\sqrt{\frac{2\rho}{\mu_0\omega\tilde{\mu}_{max}}}=\sqrt{\frac{2i\alpha_G\rho}{\mu_0\omega_M}}=\sqrt{\frac{\alpha_G\rho}{\mu_0\gamma\mu_0M_s}}. \quad (28)$$

Taking $\alpha_G=0.012$, $\rho=1.22\times10^{-6}$ Ωm, $\mu_0M_s=0.8$ T (typical values for microwire of this composition), and $\gamma/2\pi=28$ GHz/T, one obtains $\delta_{\min}=0.288$ μm. Then, the theoretical maximum of GMI ratio

$$\left(\frac{Z_{zz}}{R_{dc}}\right)_{max}\approx\frac{a}{\delta_{min}}, \quad (29)$$

as $\sin^2\varphi_m\approx1$. For microwire with radius a of 10.7 μm, $Z_{zz}/R_{dc}=37$.

On the other hand, when $H_E=(H_A\sin2\alpha)/2$, $\varphi=0$ and Eq. (26) reduces to

$$\frac{Z_{zz}}{R_{dc}}=\frac{a}{\min(\delta_0,a)}, \quad (30)$$

$\delta_0=120$ μm at 10 MHz which is much higher than the wire's radius a. Therefore, $Z_{zz}/R_{dc}=1$ as the current flows through the whole volume of the wire. Similarly, Z_{zz}/R_{dc} approaches unity at sufficiently high fields where $\tilde{\mu}\to0$ and $\varphi\to\pm90°$.

For a given microwire, the theoretical maximum of GMI effect should be more than 3000%, that is about ten times larger than this value for our sample [see Figs. 8(b) and 8(c)]. Such large difference, in agreement with Kraus,[23] is attributed to nonzero angle α that prevents achieving the resonance condition at low and moderate frequency ranges. The minimum driving frequency ω_c for which the theoretical limit of GMI can be achieved as follows:

$$\omega_c^2\approx3\omega_M\gamma H_A(\alpha/2)^{2/3}. \quad (31)$$

Subsisting $H_A=108$ A/m and $\alpha=25.5°$, one gets $\omega_c/2\pi=1.1$ GHz. This estimated minimum frequency ω_c was experimentally confirmed for the given microwire.[13]

VI. CONCLUSIONS

We developed a mathematical model for magnetization reversal and MI field dependence for zero-magnetostrictive amorphous microwires with consideration (i) for low-field ($H_E<H_A$) hysteresis which arises from deviation of the anisotropy easy axis from transversal direction and (ii) for the effect of circular bias magnetic field H_B produced by current I_B running through the wire on hysteresis and asymmetry of the MI dependence. The validity of the model was confirmed by the experiments. The nature of low-field hysteresis and its dependence on circular magnetic field were investigated. It was demonstrated that the low-field hysteresis originates from a nonzero angle between the anisotropy easy axis and transversal plane and that the application of the bias field leads to suppressing this hysteresis. Using the developed model, the main characteristics of the studied ferromagnetic microwire such as anisotropy field H_A, angle between the anisotropy easy axis with the transversal direction α, and Gilbert damping constant α_G were obtained.

ACKNOWLEDGMENTS

The work was supported by the Ministerio de Ciencia e Innovacion (Spain) under Project MAT2007-66798-CO3-01, by EU ERA-NET program under Project DEVMAGMI-WIRTEC (MANUNET-2007-Basque-3) and by the Basque Government under Saiotek 08 METAMAT project. A. Zh. and V. Zh. wish to acknowledge the support of the Basque Government under Program of Mobility of the Investigating Personnel of the Department of Education, Universities and Investigation (Grants MV-2009-2-21 and MV-2009-2-24). A. Zv. acknowledges support from the Ikerbasque Foundation.

*mihail.ipatov@ehu.es

†Present address: A. M. Prokhorov General Physics Institute of RAS, 119991 Moscow, Russia.

[1] L. V. Panina, K. Mohri, T. Uchiyama, M. Noda, and K. Bushida, IEEE Trans. Magn. **31**, 1249 (1995).

[2] K. Mohri, T. Uchiyama, L. P. Shen, C. M. Cai, and L. V. Panina, J. Magn. Magn. Mater. **249**, 351 (2002).

[3] L. V. Panina and K. Mohri, Appl. Phys. Lett. **65**, 1189 (1994).

[4] A. Zhukov and V. Zhukova, *Magnetic Properties and Applications of Ferromagnetic Microwires with Amorphous and Nanocrystalline Structure* (Nova Science Publishers, New York, 2009).
[5] V. Zhukova, A. Chizhik, A. Zhukov, A. Torcunov, V. Larin, and J. Gonzalez, IEEE Trans. Magn. **38**, 3090 (2002).
[6] M. Ipatov, V. Zhukova, J. M. Blanco, J. Gonzalez, and A. Zhukov, Phys. Status Solidi A **205**, 1779 (2008).
[7] A. F. Cobeño, A. Zhukov, J. M. Blanco, V. Larin, and J. Gonzalez, Sens. Actuators, A **91**, 95 (2001).
[8] O. Reynet, A.-L. Adenot, S. Deprot, O. Acher, and M. Latrach, Phys. Rev. B **66**, 094412 (2002).
[9] D. P. Makhnovskiy and L. V. Panina, J. Appl. Phys. **93**, 4120 (2003).
[10] D. P. Makhnovskiy, L. V. Panina, C. Garcia, A. P. Zhukov, and J. Gonzalez, Phys. Rev. B **74**, 064205 (2006).
[11] D. Makhnovskiy, A. Zhukov, V. Zhukova, and J. Gonzalez, Adv. Sci. Technol. (Faenza, Italy) **54**, 201 (2008).
[12] H. X. Peng, F. X. Qin, M. H. Phan, Jie Tang, L. V. Panina, M. Ipatov, V. Zhukova, A. Zhukov, and J. Gonzalez, J. Non-Cryst. Solids **355**, 1380 (2009).
[13] M. Ipatov, A. Zhukov, J. Gonzalez, and V. Zhukova, *Proceedings of The Progress in Electromagnetics Research Symposium PIERS 2009*, August 18–21, Moscow (The Electromagnetics Academy, Cambridge, MA, 2009) p. 1349.
[14] K. Mohri and Y. Honkura, Sens. Lett. **5**, 267 (2007).
[15] A. S. Antonov, I. T. Iakubov, and A. N. Lagarkov, J. Magn. Magn. Mater. **187**, 252 (1998).
[16] D. P. Makhnovskiy, L. V. Panina, and D. J. Mapps, Phys. Rev. B **63**, 144424 (2001).
[17] N. Usov, A. Dykhne, A. Antonov, and A. Lagar'kov, J. Magn. Magn. Mater. **174**, 127 (1997).
[18] D. Atkinson and P. T. Squire, J. Appl. Phys. **83**, 6569 (1998).
[19] E. C. Stoner and E. P. Wohlfarth, Philos. Trans. R. Soc. London, Ser. A **240**, 599 (1948).
[20] N. A. Usov, A. S. Antonov, and A. N. Lagar'kov, J. Magn. Magn. Mater. **185**, 159 (1998).
[21] V. S. Larin, A. V. Torkunov, A. Zhukov, J. González, M. Vázquez, and L. Panina, J. Magn. Magn. Mater. **249**, 39 (2002).
[22] A. S. Antonov, N. A. Buznikov, I. T. Iakubov, A. N. Lagarkov, and A. L. Rakhmanov, J. Phys. D **34**, 752 (2001).
[23] L. Kraus, J. Magn. Magn. Mater. **195**, 764 (1999).